Experimental Investigation of Mach-Effect Thrusters on Torsion Balances

Maxime Monette [a], Matthias Kößling [b] and Martin Tajmar [c*]

[a] Institute of Aerospace Engineering, Technische Universität Dresden, Marschnerstrasse 32, 01307 Dresden, Germany, maxime.monette@tu-dresden.de
[b] Institute of Aerospace Engineering, Technische Universität Dresden, Marschnerstrasse 32, 01307 Dresden, Germany, matthias.koessling@tu-dresden.de
c Institute of Aerospace Engineering, Technische Universität Dresden, Marschnerstrasse 32, 01307 Dresden, Germany, martin.tajmar@tu-dresden.de
* Corresponding Author

Abstract

Successful interstellar venture depends on the development of propellantless propulsion with a thrust-to-power ratio much greater than a photon rocket and without the limitations of solar sails. Claims of µN thrust for Woodward's MEGA Drive, along with predicted mass fluctuations as a consequence of the Mach-Effect have initiated a few decades of table-top experiments seeking to observe variable mass and using it to generate significant propellantless thrust efficiency. However, using different thrust balances with increasing measurement sensitivity to characterize these effects resulted in a decrease in the claimed effect's magnitude. Large second harmonics begin to appear in the pre-stressed piezoelectric stack's integrated strain gauge signal, showing the vibration present at system resonances, as well as significant nonlinearity. Observation of the balance beam's oscillations reveal sub-harmonic vibration coupling and amplified vibration around electromechanical resonances of the system that can explain the transients observed in the force trace. Different piezo-actuator driving conditions are explored and an account for the different behaviors observed is made. The varying driving conditions do not significantly affect the forces observed, contrary to the theory. It is concluded that the observed effect is a result of coupled vibrations on the torsion balance.

Keywords: Breakthrough propulsion, Propellantless propulsion, Mach-Effect-Thruster, Thrust Balance

Nomenclature

a	-	Acceleration [m/s^2]
c	-	Speed of Light [m/s]
C	-	Capacitance [F]
E	-	Energy [J]
F	-	Force [N]
G	-	Gravitational Constant [N·m^2/kg^2]
J	-	Moment of Inertia [kg·m^2]
k	-	Spring Stiffness [N/m]
K	-	Calibration Factor [N/m]
m	-	Mass [kg]
δm	-	Mass Fluctuation [kg]
η	-	Clamping Efficiency [1]
P	-	Power [W]
Q	-	Mechanical Quality Factor [1]
ω	-	Angular Frequency [rad/s]
ρ_0	-	Material Density [kg/m^3]
r	-	Balance Arm [m]
t	-	Time [s]
V_c	-	Capacitor Voltage [V]
V_p	-	Piezo-actuator Voltage [V]
x	-	Piezoelectric Excursion [m]
X	-	Beam Displacement [m]
ζ	-	Damping Ratio [1]

Abbreviations

AC	-	Alternating Current
ARC	-	Austrian Research Center
CSUF	-	California State Univ., Fullerton
DC	-	Direct Current
DFT	-	Discrete Fourier Transform
DUT	-	Device-Under-Test
EMI	-	Electromagnetic Interaction
FFT	-	Fast Fourier Transform
GRT	-	General Relativity Theory
MET	-	Mach-Effect-Thruster
MEGA	-	Mach-Effect-Gravity-Assist
PEEK	-	Poly-Ether-Ether-Ketone
PZT	-	Lead-Zirconium-Titanate
RHS	-	Right-Hand-Side
SNR	-	Signal-to-Noise-Ratio
TC	-	Thermally Compensated
TUD	-	Technical University, Dresden
VNA	-	Vector Network Analyzer

1. Introduction

One revolutionary space propulsion concept is based on engineering a mass variation in an accelerated object to generate thrust without having to carry propellant. Experimental investigations of variable mass according to Woodward's definition of the Mach-Effect date back to 1990: the weight of capacitors, thought to fluctuate due to discharge cycles, was closely monitored by a magneto-resistive force sensor and led to equivocal results [1]. Since then, both the embodiment of the Mach-Effect device and claim have been refined: only objects to which an external, non-gravitational force is applied and whose internal energy is varied will have its mass fluctuate according to the Mach-Effect [2]. Then, in order to create a steady thrust for space propulsion, an actuator must simultaneously push or pull the fluctuating mass. In the original patent, a thruster built from a capacitor in which a mass fluctuation is generated through discharge cycles and then accelerated by a piezoelectric actuator [3]. The latest design iteration consists in a multi-layer piezo-ceramic stack composed of lead-zirconium-titanate (PZT) disks sandwiched between two different masses and driven by a sinusoidal voltage signal. A thrust-to-power ratio of 100 nN/W is predicted for the device, as opposed to P/c for a photon rocket (3.3 nN/W), as well as scaling up potential with frequency, material selection, and array disposition [4]. According to one critic of the theory, the derivation of the mass fluctuation formula is incompatible with Einstein's field equations, since Woodward obtains second order components of the gravitational potential through Maxwellian gravity [5]. Despite the debatable assumption, Woodward's derivation leads to a measurable and transient variation of an object's mass that can be examined in laboratory experiments. However, the difficulty in scaling up the concept over the past few years blatantly points at the lack of understanding of the effect observed [6]. This paper discusses experimental results of Mach-Effect-Thrusters (MET), or Mach-Effect Gravity Assist (MEGA) drives, on sensitive torsion balances. Recent experimental results disagree with the theory developed by Woodward and the experimental artefacts are characterized, building up on previous test campaigns [7]. First, a brief overview of the theory is necessary to understand the development of the current embodiment of the experiments and to explain the selected driving conditions. Then, previous experimental results published in the peer-reviewed literature are summarized and compared, followed by an examination of the actual replicator test setup. As part of the analysis, the devices obtained from Woodward, as well as the electronics, will be scrutinized under different test conditions. The background noise is carefully investigated, spectra are obtained by sweeping the driving frequency and examining input current, voltage and embedded strain gauge signal waveforms. Moreover, the nonlinearity in the devices is investigated as well as resonance modes and vibration transmission across the balance beam. The experiments are shown to disagree with different aspects of Woodward's theory and intended thruster concept, and the force traces observed on the balance can be explained by vibrational artefacts.

2. Literature Review

2.1. Theoretical background

Observable examples of gravitomagnetic interactions such as the Lence-Thirring dragging as being a consequence of the Mach's principle in General Relativity Theory (GRT) have already been examined by Nordvedt using a linearized version of GRT and a gravitational vector potential [8]. That same method allowed Sciama to reach the conclusion that inertia was essentially the action of the distant matter of the universe [9]. Woodward started with Sciama's argument to derive the mass fluctuation equation seen below. Although the influence of the external force, or acceleration, is not explicitly shown, the local mass fluctuation as a function of time $\delta m(t)$, seems to be a consequence of varying internal energy E, due to an applied force. Equation 1 give the mass fluctuation, and an alternative is found at p.94, with the full derivation pp.82-86, in Woodward's book "*Making Starships and Stargates"* [2] , where c is the speed of light in vacuum, ρ_0 the object's proper density, and G the universal gravitational constant:

$$\delta m(t) = \frac{1}{4\pi G}\left[\frac{1}{\rho_0 c^2}\frac{\partial^2 E}{\partial t^2} - \left(\frac{1}{\rho_0 c^2}\frac{\partial E}{\partial t}\right)^2\right] \qquad \text{Equation 1}$$

Figure 1 illustrates the conceptual design of the MET as described in Woodward's original patent where a varying mass, generated in a capacitor according to Equation 1, is swung back and forth by an actuator attached to a spacecraft to produce thrust in free space. Woodward recognizes that the electrostatic energy may not entirely contribute to internal proper energy change but states that it may be a good starting point for an analysis [10]. In this case, the resulting mass fluctuation, obtained from the larger, first term on the RHS of Equation 1, is proportional to the second derivative of the capacitor's electrostatic energy, $E = \frac{CV_c^2}{2}$, with capacitance C and voltage V_c. Thus, the effect should occur at twice the driving frequency ω and scale with its square, according to Equation 2. With an applied field $V_c \sin(\omega t)$, for instance:

$$\delta m(t) = \delta m \cos(2\omega t) = \frac{CV_c^2\omega^2}{4\pi G\rho_0 c^2}\cos(2\omega t) \qquad \text{Equation 2}$$

Any actuator can be employed to move the capacitor to and fro in converting the fluctuation into a static effect using Newtonian mechanics, in Equation 4 below. For a piezoelectric actuator, the elongation x depends on the applied voltage V_p, a piezoelectric coupling constant in the direction of polarization d_{33}, and is reduced by a factor η due to mechanical clamping [11]; at resonance, the excursion can be amplified by a quality factor Q, as shown in Equation 3. With the excursion chosen at twice the capacitor's driving frequency, and at resonance,

$$x(t) = x\cos(2\omega t + \varphi) = \eta Q V_p d_{33}\cos(2\omega t + \varphi) \qquad \text{Equation 3}$$

Woodward then used Newton's first law, $F = mdv/dt$, considering a variable mass and the second time derivative of the piezoelectric excursion, where averaging over one cycle leaves one term standing:

$$F_{avg} = \frac{\omega}{2\pi}\int_0^{\frac{2\pi}{\omega}} \delta m(t)\ddot{x}(t)dt \qquad \text{Equation 4}$$

, which results in a static force,

$$F_{avg} = \frac{\omega^4 CV_C^2 V_p \eta Q d_{33}}{2\pi G\rho_0 c^2}\cos\varphi \qquad \text{Equation 5}$$

The actuation force should act at twice the frequency of the capacitor's driving voltage in order to be in phase with the mass fluctuation and produce net thrust: pulling the mass when it is heavier, and pushing it when it is lighter, for instance. A significant parameter is the phase difference φ between the actuation and the mass fluctuation, and material parameters such as the quality factor at resonance and clamping stiffness. The expected thrust is now proportional to the driving frequency to the power of four, and should be significantly increased by augmenting the voltage to the capacitor, the driving frequency, and also by enhancing the actuating signal at twice the driving frequency, according to Equation 5.

Detractors of Woodward's theory mention that the higher order effects considered in Equation 1 cannot be obtained from a linearized theory of General Relativity [5,12]. In addition, since Sciama was incapable of continuing his derivation in full tensor form and ensure Lorenz invariance, his result, also used in Woodward's derivation, might not be consistent with Einstein's field equations in the first place [13]. Brans also noted that inertial induction or Mach's principle in Einstein's construct was purely a coordinate effect that should have no detectable consequence, which also seems to go against Woodward's derivation [14]. In a later paper, however, Fearn pursues with arguments from Hoyle and Narlikar to derive Woodward's mass fluctuation equation and reaches the same result as Woodward, apart from a small numerical factor [15,16]. Hence, experiments were conducted to reach a definitive answer.

2.2. Experimental background

In 1996, the set of experiments conducted with Woodward's patented design showed the weight measured over time as the capacitor and PZT actuator were powered [17]. Distinct phase differences between the capacitor and actuator driving signals were tested (0°, 90°, 180°). In one example, a capacitor undergoing mass fluctuation was driven with 140 W at 5.5 kHz, and the actuator was driven with 10 W and a frequency doubler. The reported mass change was around 1 mg (67 nN/W), however, the signal-to-noise ratio (SNR) was very low and the standard deviation between the measurements not stated. The major effect observed was about two orders of magnitude greater than the supposed mass change and was explained by a change in the spring constant of the measuring device: thus, assuming the presence of a nonlinearity in the vibration, the results were far from being conclusive.

With a novel design iteration termed the Mach-Lorenz Thruster, Woodward aimed to increase the operating frequency and therefore the observed effect, by accelerating the capacitor using the lattice restoring force of an inductor instead of a PZT actuator [18]. In these tests, the driving frequency was 50 kHz, the power to the inductor 300 W and to the capacitor 2.5 kW. The SNR in these results was even lower than in previous research, although a thrust force of 100 µN was claimed after averaging 200 cycles. The obtained, theoretical thrust-to-power ratio also sank to 40 nN/W. The experiment was later repeated by Buldrini et al. [19] using a µN-resolution torsion balance and higher driving frequency, only to obtain a smaller test result: the capacitor and inductor power had amplitudes of 6 kW and 1 kW respectively, while an effect under the balance noise of around 30 µN could not be resolved (4 nN/W). Since the same force was observed in the dummy test where power was fed to the inductor but the capacitor was disconnected, the effect was attributed to an experimental artefact. Research using this iteration was later abandoned by Woodward, pp.118-146 [2].

The third and most recent iteration of the Woodward thruster has the mass fluctuation being generated in the pre-stressed piezo-ceramic stack itself as it is expanded and compressed electromechanically with the applied voltage. The MEGA drive (Figure 2) is a multi-layer piezoelectric disk stack that is compressed between an aluminum disk and a brass cylinder of the same diameter using stainless steel screws. Also, a thin, passive piezoelectric disk embedded in the stack is used as a strain gauge to provide a relative measurement of the stack's vibration amplitude and its phase relative to the applied voltage. The necessary actuation that transforms the transient mass fluctuation into a static force is supposedly produced by a nonlinear effect within the stack, which Woodward identifies as electrostriction. A few simple models have attempted to make thrust predictions for the proposed concept, and state a dependency of thrust on the driving frequency to a power of six, and to the voltage to a power of four [20,21]. However, these models do not take into account the strength limitation of the piezoelectric materials, quality factors at resonance, and the contribution of the vibration of other important masses in the balance setup [22]. Most importantly, the calculation is complicated by the existence of different forms of nonlinearity and the lack of knowledge of their magnitude and relative phase to the first harmonic signal.

Recent publications from Fearn show a maximum effect of 2 µN (40 nN/W) [6]. In the average of the forward and reverse runs, in Figure 3, the force profile on the left shows an impulse at switch-on and another at switch-off in the opposite direction. The force measurement resulting from a constant driving frequency signal results in a steady force in the opposite direction to the switch-on transient that does not exceed it in magnitude. The voltage does not stay constant over the pulse and present spikes in some instances. When using a different device, amplifier and driving frequency, the magnitude of the effect does not vary significantly (right), and although the switching transients are still present, the observed force during the profile drifts in another direction. The absence of a balance and voice coil calibration in the California State University, Fullerton (CSUF) publications from Woodward et al. led to a recent investigation by Hathaway [23], which helped to conclude that the results reported thus far should be reduced by a factor of at least four: leading to a thrust-to-power ratio of 10 nN/W in retrospective.

These tests were first repeated by Buldrini on a torsion balance in vacuum at FOTEC, Austria, with a device received from Woodward in 2014 [24]. The driving frequency was slightly different than Woodward's (40 kHz) and was selected to produce the largest effect. The results in Figure 4 show a similar force signature on the balance as obtained by Woodward, an order of magnitude lower. There are sharp switching transients, and what appears to be a small steady force during the pulse of the forward measurement (left). Also, the behavior is flipped when the device's orientation is rotated by 180° in the reverse measurement (right). One observes, however, a very low SNR, examined over pulses of 7 s, which approaches the balance's reaction time and is a bit short to claim steady-state forces. Then, the experiments were replicated by Tajmar et al. at the Technische Universität Dresden (TUD) also in vacuum and on torsion balances [7,25,26]. On a previous version of the balance (V5), tests with an old device from Woodward using resonance frequency tracking and a 75 V peak amplitude signal resulted in a force of around 0.4 µN that didn't reverse when changing the orientation of the device within the test box, which pointed at electromagnetic interaction and at a thermally induced center of mass shift [25]. Subsequently, in an attempt to amplify the effect by increasing the actuating signal (see Equation 3), mixed voltage signals combining single and double frequency components with various relative phase angles were applied. This didn't result in more force, but small switching transients remained [7]. Even with a second type of vibrating actuator, using magnetostriction to generate greater vibrational amplitude, the transient forces observed were not of the magnitude predicted by the theory [7]. On one hand, adding a transformer to the electronic setup slightly increased the effect observed, but the dummy test results with a resistor and AC current showed a similar effect that hinted at electromagnetic interaction [7]. Thus, the experiments were repeated with an improved setup; the actual torsion balance (V6) offers greater measurement accuracy, proper grounding and better electromagnetic shielding. A device of the same model provided by Woodward (NS5) was tested at various frequencies using Woodward's amplifier and transformer; the effects observed at a constant driving frequency were even smaller than before, not exceeding 200 nN [26]. Hence, the experiments so far do not seem to point at the existence of a Mach-Effect as described by Woodward, but they do constitute an interesting electromechanical problem which will be studied in greater detail using a setup closer to Woodward's.

3. Experimental setup

Consequently, based on Woodward's device and electromechanical setup as tested at CSUF from 2012 to 2019 [27,28], the experiments were replicated and investigated under different test conditions in order to explain the origin of the force profile observed. The original setup and device from Woodward are tested, and the results are compared with other setups and test parameters. In this section, the mechanical and electrical setups are described.

3.1. Balance setup

The basis for the measurements is a torsion balance that has undergone various improvements over more than 4 years, illustrated in Figure 5 and placed in a large vacuum chamber (0.9 m diameter, 1.5 m length). A thrust produces an angular displacement that can be measurement by a laser interferometer. The Fabry-Pérot type interferometer, IDS3010 from attocube, has a sampling rate as high as 10 MHz and a position measuring resolution of 1 pm with an average noise of 1-2 nm at room temperature [29]. Then, along with the length of the balance arm, the balance pivot determines the force amplification factor and is composed of two C-flex A-20 torsion springs with low torsional spring rate (each 3.3 mN·m/°) and low hysteresis, to achieve repeatable sub-µN resolution while supporting enough weight on the balance arms. A balance calibration is performed using a voice coil from Moticont (LVCM-010-013-01) with high linearity, and a Keithley 2450 source meter, also with high accuracy and sub-nA resolution for precise current control.

The calibration of the voice coil calibrator is first performed on a weighing scale with 0.1 mg resolution (Sartorius, M-Pact AX224) by commanding precise forces with the current source, as the gap between the coil and magnet is varied (Figure 6, left). The voice coil calibration results determine the force to current conversion factor, and the gap length is selected between 2 and 4 mm where the factor deviation is minimal [7]. The balance is then calibrated by commanding a wide range of currents to the voice coil and observing the generated displacement of the balance beam using the attocube. The balance calibration results in a high degree of linearity and determines the conversion factor relating the force to the beam displacement (Figure 6, right). A shorter version of this balance calibration is performed before and after every series of tests. Furthermore, the balance beam's motion is slightly damped by an eddy-current brake consisting in a pair of neodymium magnet disks secured to the balance beam and enclosing a copper plate fixed to the rest frame, whose height can be adjusted to influence the level of damping. Figure 7 shows an example of the balance's reaction to a commanded voice coil pulse: the steady state force achieved after single overshoot exactly reaches the commanded force with a total delay of 15 s. The figure also shows that the torsion balance can be approximated to a 1D simple harmonic oscillator with moment of inertia J, balance arm r, a spring stiffness K of 0.2 N/m and a damping ratio ς of 0.85, by solving the equation of motion below for the beam displacement X.

$$\frac{J}{r^2}\ddot{X} + 2\varsigma\sqrt{\frac{J}{r^2}K}\dot{X} + KX = F_0 \sin(\omega t) \qquad \text{Equation 6}$$

Amplifiers and oscilloscopes are located outside the vacuum chamber to minimize electromagnetic interaction (EMI), and power and data signals are communicated to the device on the balance using Galinstan liquid contacts located at the balance's central pivot to remove any torque from cables to the balance beam. The vacuum chamber uses a vibration-isolated Edwards XDS35i scroll pump and a Pfeiffer 2300 L turbo-pump to reach a vacuum down to the 10e-7 mbar range. The experiments were performed at room temperature and in medium-vacuum using the scroll pump (10e-2 mbar). Finally, Table 1 compares the TUD balance to the CSUF balance: a better force resolution comes at the expense of a slightly greater reaction time.

3.2. Electronics setup

Although a set of high-power amplifiers dedicated for piezo-actuators were initially employed as part of the TUD setup, the experiments were repeated using the original equipment from CSUF. The block diagram in Figure 8 gives an overview of the electronics setup used. In both cases, an input voltage at a specific frequency is provided by the frequency generator (Picoscope 5442 B). The signal is then amplified outside the vacuum chamber to reduce thermal effects and EMI on the balance. The voltage applied to the device and the strain gauge voltage signal are read by the digital oscilloscope using differential probes, whereas the applied current is read using a Hall sensor (JA4635, Coilcraft). The command signal is monitored as a reference by the oscilloscope as well. The CSUF setup is intended to replicate the electronics used by Woodward in most of his experiments [20], before the recent change to an ENI 2100L RF amplifier and 2:1 transformer [6]. The main difference between the TUD and CSUF setups lies in the type of amplifier used, as well as a 4:1 step-up transformer between the amplifier and the MET to modify the load impedance in the CSUF setup. Both setups were tested and characterized.

From the Bode plots obtained in Figure 9, the D-class amplifier (APEX PA04) used in bridge-mode shows a constant amplification of 200 over its whole frequency spectrum for a resistive load as well as for the unloaded case. In the case of the A/B-class amplifier (Carvin DCM1000), the Bode plot is slightly different: the amplification and phase change are not linear over the frequency spectrum examined, and only the unloaded case is shown. It should be noted that the output signal is specified only until 20 kHz and only for specific load impedances of 4 or 8 Ω by the manufacturer [30].

The experiment profiles are automated using a dedicated LabVIEW program and personalized scripts structured into sectors. In the case of a fixed frequency profile: after a period of inactivity (sector 1), the frequency and input voltage are ramped up to the commanded value within 0.1 seconds (sector 2) and maintained constant for 16 seconds during the pulse (sector 3), followed by a ramp down of the command signal to zero within 0.1 seconds (sector 4) and a period of inactivity (sector 5). The periods of rest were set to 30 minutes to allow the device to cool down between the experiments. Applied voltage, device temperature, applied current, driving frequency, chamber pressure and strain gauge voltage signals are all read at a frequency of 10 Hz, unless otherwise stated. The automated scripts allowed several profiles to be executed during the night to avoid external disturbances, and be carried out with the same setup to get an average of a significant number of identical test runs. Lastly, in frequency sweep tests, the driving frequency starting at 24 kHz is raised to 48 kHz by increments of 50 Hz every 20 ms during the pulse (sector 3). Driving frequency sweeps were individually and manually executed with the digital oscilloscope in a few exceptions.

3.3. Electromechanical test setup

The NS5 device, MET of the same series as NS7 and NS11 according to CSUF terminology, was obtained from Woodward in January 2019. Each stack is built manually using SM111 (PZT4/Navy II) disks from Steiner and Martins, Inc., brass electrodes, and epoxy joints as well as an alignment jig. The device is illustrated in Figure

10 along with parts descriptions. The piezo-disks are mechanically connected in series and electrically connected in parallel to maximize piezoelectric excursion. Also, the strain gauge and the piezo-stack share a common ground, which is conducted through the screws and bracket of the device. The MET is attached to the experiment box using a single screw and nylon washers to help damp vibration, and separated by a plastic plate (PEEK) to electrically isolate the device from the balance. The box is a grounded Faraday cage composed of mu-metal, to reduce stray electromagnetic fields, and is fixed directly to the balance beam. In specific cases, Woodward's own 'vibration-isolating yoke', constructed using acrylic plates and O-rings aiming to damp vibration, was used along with a different Faraday cage to attach the device to the balance beam. Table 2 summarizes the device dimensions, whereas the only difference between NS5 and NS7 lies in the machining of the L-bracket. Each screw was tightened and regularly checked using a torque wrench, to 4 lbf-in (0.45 Nm).

The resonance spectrum can be obtained by examining the strain gauge signal when applying a low voltage, and the impedance spectrum can be obtained precisely by using a vector network analyzer (VNA), i.e. Agilent 4294a, or by examining the current for an applied AC voltage. The resonances were also examined using the laser interferometer targeting the device's end masses, both brass and aluminum were used as reflective targets while the device was fixed on an optical table (Figure 11). The vibration of the end masses were observed on an older device, also received from Woodward, baptised WT03 and having a similar build to NS5. Lastly, the temperature increase of the device was assessed by fixing a K-type thermocouple with a piece of Kapton tape to the brass mass. However, this temperature measurement method is limited, as it does not give a direct indication of the temperature inside the piezo-ceramic itself.

4. Electromechanical analysis

4.1. Spectral analysis

Characterization of the devices using spectral analysis is essential to selecting the test driving frequencies, allowing a comparison between individual runs, and understanding the effects seen on the torsion balance. METs may all have a similar build, however, since PZT disk manufacturers specify a 15-20% standard deviation in the material properties and resonance of the disks, and the stacks being composed of eight PZT disks can end up having an important deviation to one another [31]. Furthermore, pre-stress can have a significant effect on the stack behavior and the uncertainty in the screw-tightening procedure with a torque wrench can be up to 20% for each of the six screws on the stack side [32]. The resonances of a piezoelectric stack shown in a VNA sweep are electromechanical and are as much influenced by the mechanical conditions: clamping, geometrical configuration, material stiffness, as they are by the electrical configuration: applied electric field, loads connected in series or parallel [33]. The spectrum obtained with an impedance analyzer occurs at very low voltage and stress levels, and offers an unloaded spectrum of the device since it is disconnected from any additional electrical load such as a transformer or an amplifier. In the case of the loaded spectrum, a sweep of the driving frequency is performed at a fixed voltage or current, and the device is connected to the balance, amplifier and sensor electronics.

On one hand, the loaded spectrum is the most relevant for these experiments, as it identifies the resonances of the system as tested on the balance with the integral experiment setup. Figure 12 shows the effect of the electrical setup, responsible for signal amplification. The curves are obtained by performing a Fast-Fourier-Transform (FFT) of every waveform during the driving frequency sweep, and logging the magnitude of the main frequency component, the first harmonic. One observes, that the load impedance is not constant and is characterized by more than one resonance. And although the mechanical setup is identical in both tests, the electronics modify the frequency spectrum significantly. First, the CSUF electronics are more subjected to noise, as can be seen from the fluctuations near resonance, where the first harmonic signal was polluted by higher frequency components. Second, as expected when comparing amplifiers' bode plots, the CSUF electronics (right) introduce a new resonance in the system around 35 kHz, which is not seen in the loaded curve with the TUD electronics (left). Also, the resonance represented by the impedance dip at 33 kHz is weaker for the CSUF setup. Third, the strain gauge signal curve shows the forces in the device where the peaks correspond to the impedance dips seen in the TUD spectrum. The strain gauge signal usually closely follows the current curve, which means that the vibration in the device driven at constant voltage is mostly proportional to current. However, the peaks observed in the strain gauge signal curve of the CSUF spectrum do not always correspond to an impedance dip (i.e. 29 kHz); the electronics are most likely responsible for this behavior. Lastly, the vibration level at 36 kHz is three times higher for the CSUF than for TUD, even if the respective currents show an anti-resonance mode, a mode of high impedance. Thus, we expect these differences, based solely on the electronics setup, to be translated to different behavior in terms of vibration and power transmission to the device. Also, since the strain gauge signal follows the current and shows resonance behavior in a fixed voltage sweep, an unloaded spectrum for a comparative analysis can be obtained solely by looking at the strain gauge signal at low voltage without the need of an expensive impedance analyzer.

On the other hand, the unloaded spectrum is a simple way of characterizing the device itself, independent of external influence, to examine the effects of ageing, screw loosening or other types of degradation. Figure 13 compares the unloaded spectrum of NS7 for different conditions, as obtained solely from the strain gauge signal to driving voltage ratio at low voltage (left). The Device-under-Test (DUT) is placed on the balance and mounted using Woodward's yoke. The resonances represented by signal peaks visibly vary due to the device's temperature, possibly due to degradation, and when placed in vacuum, by a few 100 Hz. Several concurrent conditions may modify the spectrum obtained due to the high number of screws, parts and layers: the resonance may be influenced by the looseness of any screw resulting in inhomogeneity of the preload stress, by ageing and the degradation occurring in the piezoelectric material itself, and lastly, by the temperature of the device as an indication of losses in varying driving conditions. A simpler piezoelectric object would be required to examine the effect of each individual conditions. Figure 13 shows, for instance, the influence of driving voltage on the resonance spectrum: the increase in frictional losses results in a smaller strain gauge signal, as well as a shift in the resonance frequency. This analysis shows the presence of several system resonances, the difficulty of maintaining specific driving conditions at a fixed frequency, and the occurrence of a frequency shift at higher driving voltages.

Lastly, examining the second harmonic content of the measured signals provides relevant information, since Woodward stresses the importance of nonlinear vibration in actuating the mass fluctuation to generate steady thrust [20]. In Figure 14, the second harmonics of the current and strain gauge signal are plotted against the x-axis representing the driving frequency to show the relation to the impedance spectrum in Figure 12. The magnitudes of the second harmonic components were obtained by taking the second highest frequency peak in the Discrete-Fourier-Transform (DFT) of the signal waveforms. A strong nonlinear effect is shown representing up to 6% of the linear piezoelectric signal around resonance. This effect was attributed to electrostriction by Woodward and Buldrini, however, electrostriction is known to be only a small nonlinear contribution in perovskite ferroelectrics such as PZT [34]. The second harmonics observed are more likely due to other nonlinearity present in piezoelectric material, such as the contribution of domain wall motions, which increase at higher driving voltage [35–37]. The second harmonic DFT of the strain gauge signal shows that the driving frequency for maximum nonlinearity depends on the electronics used: again, the CSUF setup curiously shows the 36 kHz frequency peak, whereas in the TUD setup, the nonlinearity optimum corresponds to the resonance around 33.5 kHz. As a consequence of this analysis, different driving frequencies can be selected for both setups: in the range where resonance and high second harmonics occur.

4.2. Vibration analysis

Polishing the aluminum and brass surfaces of the device provided enough reflection to quantify the movement of the head (aluminum) and tail (brass) masses using a laser interferometer during a driving frequency sweep at constant voltage with the device's bracket fixed to an optic table. The vibration amplitudes in the frequency domain were obtained using DFT and were plotted in Figure 15, to illustrate two important points. The figure on the left, obtained by plotting the first harmonic content of the signals against the driving frequency, shows that the brass mass vibrates almost as much as the aluminum mass at resonance regardless of the rubber pad. This defies the purpose intended by Woodward and indicates that the device is not designed to create maximum thrust; optimally, the tail mass should undergo minimal movement so that most of the energy is transmitted to the head mass. The figure on the right shows a DFT of the vibration signals at a specific driving frequency (34.5 kHz) and reveals that the brass-side vibration contains more second harmonic content than the aluminum mass side. This indicates that the piezoelectric vibrations, both first and second harmonic content, will be transmitted to the experiment box and to the balance beam since the connection to the tail mass is rigid and rubber damping seemingly inefficient in this configuration and at these frequencies. Furthermore, it suggests that a mechanical nonlinearity could stem from the brass side of the device itself: slipping in the screw connection to the bracket, or from the bracket connection to the beam. The DFT spectrum bins are wide due to the low sampling rate selected during the experiment but showcase the important nonlinearity present in the device around a resonant vibration mode nonetheless.

5. Torsion balance test results

5.1. Function test results

The torsion balance was calibrated with pulses of different magnitude and the results showing great resolution and repeatability were shown earlier in Section 3.1. Balance characterization follows with a three-axis pulse calibration using the voice-coil and different mountings to examine influence of forces directed in any other axis than the thrust axis. As is to be expected from the torsion balance's design, the detected force in the vertical and longitudinal axes represents less than 0.4% of the commanded force whereas a pulse in the thrust axis accurately reports the commanded force, as seen in Figure 16 [26]. These results show that placing any device with its thrust axis perpendicular to the balance plane, or aligned parallel to the balance beam, should not result in forces comparable to the ones obtained when the device is oriented to show thrust, as expected. Thus, an important test will be to position the device parallel to the balance beam to see if the forces produced compare to the perpendicular orientation, or if the effects seen are artifacts observed in all directions.

Then, in order to examine the possibility of false positives, the next tests consisted in applying DC and AC voltage signals, representative of thruster tests, to a resistor fixed on the balance as a dummy DUT. Figure 17 (left) portrays the force detected by the balance when the resistor is powered by AC voltage for 15 seconds, and represents an average of 10 test runs. The force trace shows the consequence of thermal drift corresponding to the resistor heating up, although no impulsive behavior is detected. The graph on the right also shows the consequence of thermal drift, but no electromagnetic effect due to a DC current. Both graphs also portray a thermally compensated force trace, showing very low noise of about a few nN and no drift. Thermal compensation (TC) was performed to remove any kind of drift by obtaining a linear fit between the data points at the start and end of each sector and subtracting this linear drift from the data in each respective sector. The resulting trace doesn't show any force. Thus, any impulse-like electromagnetic artefact associated with a DC current in the order of 0.8 A applied to a 18 Ω resistor, or from AC voltage of around 110 V peak amplitude applied to a 470 Ω resistor, should have been eliminated through grounding the balance beam, the use of mu-metal plates covering the balance beam and experiment boxes, and co-axial cables for the balance's power feedthrough. These measurements are important since they examine similar conditions to the MET driving conditions and discount the electromagnetic forces as an explanation for forces observed on the balance beam.

5.2. MET test results

The first torsion balance MET experiments were performed in conditions coming as close as possible to Woodward's setup using CSUF electronics. NS5 is enclosed in a grounded Faraday cage to reduce its electromagnetic interaction with the surrounding structure, and is fixed directly to the balance beam. In one case, however, the device was placed in a non-grounded Faraday cage and connected to a yoke provided by Woodward. Several orientations were tested to examine the dependence of the effects on direction: 0° means that the device's longitudinal axis is perpendicular to the beam and in the torsional plane, and the brass mass is located on the left when looking from the device towards the balance's central pivot, then, the device is rotated by 180° while keeping the device upright and in the torsion plane, finally, 90° has the device's longitudinal axis aligned with the beam and with the brass mass towards the outside of the balance (and -90° has the brass mass closer to the pivot). For the TUD balance setup, a negative deflection of the beam is a negative force and entails a movement of the beam towards the aluminum mass with the MET placed in a 0° configuration (see Figure 5).

In the following series of graphs, a fixed input voltage to the Carvin amplifier of 600 mV was commanded for 16 seconds at a fixed frequency of 36.3 kHz, close to a resonance in the CSUF setup, and as specified by Fearn [38]. In Figure 18, each graph represents an average of two to five profiles, showing the force trace and driving voltage amplitude. One first notes that the value of the voltage amplitude is not constant over the duration of the pulse, although a fixed voltage and frequency are commanded. This is explained in the electromechanical analysis, as a consequence of device heating and relaxation of the mechanical connections resulting in a shift in the resonance frequency. Furthermore, not only is the voltage amplitude slightly different when comparing the cases where only the orientation has changed, but the behavior of the voltage also varies, with the odd occurrence of spikes or decline. This indicates that the change in mechanical connection, or clamping, when rotating the device, or after performing a couple of tests, might have slightly changed the device's impedance spectrum. Although the slightly different driving frequency, or voltage, should, in theory, have various consequences on the force, the observations show very little variation.

Woodward's force signature can be observed: what resembles opposite switching transients, and a small plateau or bump in the middle of the pulse in the opposite direction of the switch-on transient, as is also observed in Buldrini's results (Figure 4). The magnitude of the force plateau for 0° is around 120 nN and null for 180°, the net result is then between one and two orders of magnitude lower than Woodward's measurements. The switching transients for the 90° orientation are of the same order of magnitude as the other orientations, around 50 nN, but little to no plateau is detected, like for 180°. Additionally, the fourth graph shows a reproduction of the 180° orientation test, this time mounting the device on the yoke provided by Woodward. The measurement contains the same features as the measurement without the yoke, and this time a clear plateau can be seen. In all cases, the force trace does not return to its original position right away, however, this linear drift has been removed by using thermal compensation to better recognize pulse-like forces. The temperature shows a rapid increase, slow decrease, and an offset between start and end temperature, which seems to correspond to the behavior observed in the force trace when including the drift.

Figure 19 displays a collection of similar tests performed, this time using TUD electronics and a constant voltage amplitude of 180 V. The observed phenomenon is quite similar to the previous tests with the CSUF electronics, and the transients are even smaller in magnitude. In this case, although the driving voltage amplitude and frequency are maintained, the current slowly drifts downwards, and varies its behavior when changing the orientation, showing again the difficulty of obtaining identical driving conditions when simply switching the device's orientation or continuously operating the same device. The latter is heating up and relaxing, the impedance spectrum is shifting again, and screws may get loose. Roughly the same order of magnitude is observed for the switching transients though, irrespective of the orientation, and the 90° test can be disregarded since it features exceptionally low current. Furthermore, although the sign of the forces observed have seemed so far consistent with the change in MET orientation, the top left diagram for the 0° orientation has the transients in the opposite direction with respect to its counterpart in Figure 18, which casts doubt on the orientation dependency of the effect. Lastly, a driving frequency of 34 kHz was selected for a fixed frequency test with 90° orientation which resulted in ten times greater current but not in a correspondingly larger effect. In the recent CSUF publications, there has not been data published with other directions than forward and reverse (equivalent to 0° and 180°), but Woodward has published a few vertical configuration tests in his book, pp.165-166. The vertical tests actually showed switching transients with the same magnitude as for the forward and reverse runs. In these experiments, the Woodward behavior can be clearly seen in all device orientations and with different electronic equipment.

The last series of measurements shows the force trace resulting from a driving frequency sweep at a fixed command voltage using CSUF electronics only and the MET oriented at 0° and then 90°. Since the driving conditions cannot be maintained for a fixed frequency pulse, and the exact conditions for maximum force can only be targeted with difficulty, a sweep allows one to meet the optimal driving frequency for a very short duration. Furthermore, a frequency sweep allows one to examine the frequency dependency of the effect, whether if it is ω^3 or ω^4 dependency as predicted by Fearn and Woodward [20]. Figure 20 shows the commanded frequency, the brass temperature and the detected force. The graph shows how the balance swiftly reacts at a specific frequency, 33.1 kHz for the 90° orientation (right), before lashing back just about when the brass temperature spikes up. The fast temperature rise of the brass indicates the resonant vibration since it is directly associated with increased vibration amplitude, stresses in the stack and hence friction and heat generation. For the 0° orientation (left), the impulse occurs at a frequency of 35.2 kHz, around a second resonance frequency of the device in the range under consideration. Without thermal compensation, one would see that the final position is not the same as the start position, which indicates that something might be displaced by high frequency vibration, shifting the beam's center of gravity. This offset could, however, be explained by thermal expansion since the device is not symmetric and consists of parts with different thermal expansion coefficients. On one hand, performing a sweep also results in an effect of two orders of magnitude greater than the fixed frequency test, closer to Woodward's result. On the other hand, the effect is observed for both the 0° and 90° orientations with a similar magnitude, which is not compatible with the idea of a unidirectional thrust along the thruster's longitudinal axis while considering the triple-axis calibration of the balance. Furthermore, the force response to the driving sweeps clearly do not indicate any cubic or quartic dependency of the thrust force to the driving frequency, but rather singular events. These are individual measurements that were not very repeatable, as some runs didn't show any effect above the noise and the spike was not always at the exact same frequency. Again, this can be explained if the impedance spectrum of the device changes during or after the operation, and if the exact resonance is not met by the fine sweep. Even if the forces observed during the sweeps are non-negligible, which is most likely a result of being able to target the peak driving conditions more finely than the fixed frequency test, the fact that it is observed in the 90° orientation, and that the balance does not come back to its original position, are hints that it does not constitute thrust. Nonetheless, it is undeniable that the balance beam seems to move markedly under specific driving conditions.

6. Analysis of vibrational artefacts

The observations so far do not seem consistent with what has been claimed by previous experiments from Woodward, and even less by the theory. There is no evidence of even a quadratic dependency on voltage, frequency, or a second harmonic signal, the forces are much lower than predicted (3 to 30 nN/W), and are present in thruster orientations that should not result in thrust. The optimal driving conditions seem difficult to accurately pinpoint, however, the sweeps demonstrate a greater effect, worthwhile to examine.

Thus, the sweeps were repeated and analyzed in greater detail: first, a sweep is performed with NS7 mounted using Woodward's yoke and driven using TUD electronics, allowing a more stable signal and lower noise. Moreover, the beam displacement is observed by the laser interferometer and its analog output with an increased sampling rate of 0.12 to 1 MHz, as opposed to the usual 10 Hz read by the LabVIEW program. Figure 21 shows the result of a Discrete-Fourier-Transform (DFT) of the current and beam vibration signals at one specific driving frequency (35 kHz) during the sweep. The current trace shows a high peak at the driving frequency, and a second peak at twice that frequency representing the nonlinearity, which agrees with the analysis of the MET at resonance so far. The nonlinearity is of electromechanical nature, and stems from the mechanical construction of the device as well as from the nonlinear piezoelectric properties of the PZT ceramic disks, as examined in section 4. In the beam vibration signal, a significant peak with an amplitude of 10 nN is seen at 500 Hz, as well as one of much lesser significance at twice the driving frequency. Thus, the yoke doesn't seem to isolate these vibrations completely.

Then, the first harmonic component of the current and the beam vibration amplitude at 500 Hz obtained from the DFT were plotted over the driving frequency sweep. Figure 22 shows sweeps performed with NS5 at a 90° orientation, without the yoke, driven with TUD electronics (right) and CSUF electronics (left) while observing the beam vibration with a 200 kHz sampling rate. The same 500 Hz vibration peak was observed using both setups, regardless of the driving frequency inducing the vibration. The vibration only appeared at a few specific frequencies as can be seen in the graphs. With the TUD electronics (right), the vibration peak only appeared closely after the first resonance peak was swept through. With the CSUF electronics (left), the vibration peaks occurred more sporadically due to erratic behavior of the electronics with the piezoelectric load. These measurements are a strong indication that the device's vibration couples with the vibration of a part in the balance that is connected to the beam. Lastly, Figure 23 shows that this transient vibration is even present in a fixed frequency run. In the DFT of a few current and beam vibration waveforms for NS7 driven using CSUF electronics and mounted on a yoke at 0° orientation, the beam vibration at 500 Hz is at its maximum when switching the power on. The beam vibration comes and goes as the driving conditions slightly fluctuate, as seen previously in fixed frequency tests. Hence, there is definite evidence of transient beam vibration, linked with the force peaks observed in the figures above. As mere speculation, it is possible that a strong, high-frequency vibration can excite a bending mode of the torsional spring used as the balance pivot.

Moreover, additional experimental observations seem to indicate the presence of strong vibration, not only on the side of the PZT stack and the head mass, as conceived, but also on the side of the bracket that is fixed quite rigidly to the balance beam. First, brass powder deposits distributed under the brass mass have been observed in the Faraday cage after experiments. Also, regularly checking the torque on all screws has led to the observation that the screws on the bracket side tend to loosen every few tests, in contrast to the screws on the side of the aluminum mass. The effects mentioned are certainly a result of vibration in the stack, and could be mitigated by using the same material for the screws and the end pieces.

Now, in an attempt to answer the question whether a linearly or nonlinearly sinusoidal oscillating device on a quasi-frictionless pivot should produce any observable net displacement, the balance was modeled using a 1D simple harmonic motion (SHM) oscillator, and the piezoelectric device, as a sinusoidal forcing function. Then, solving the differential equations given by the equation of motion (Equation 6) for the SHM with a sinusoidal forcing function at 1 Hz, the resulting force trace was obtained in Figure 24 (right). The figure on the left shows the experimental results obtained when applying a sinusoidal force to the balance beam at a frequency of 0.5 Hz using the Keithley 2450 and the voice coil. Both results seem to agree with each other: the forcing function can be seen in the force trace if its frequency is low enough, and the switching transients are clearly visible. Are the switching transients observed in the experiment simply explained by this oscillation? Since the driving frequencies are much higher than the frequency considered here, what will the force trace look like? Figure 25 reveals other interesting facts: as the forcing frequency is increased, the magnitude of the switching transients is reduced but still visible, even though the forcing frequency is no longer perceptible in the force trace. Thus, the ratio of the switching transient amplitude to the forcing function amplitude should be very low for a signal of 35 kHz or even 500 Hz. However, if the sampling rate or the resolution of the laser interferometer are improperly selected, it is possible to observe the overall beam displacement as a switching transient but completely miss the beam oscillation at the forcing function's high frequency.

Hence, the switching transients can be explained by simple linear oscillation and Newtonian mechanics, however, the simulation results do not show a static force during the pulse: the linear oscillation cannot explain a steady force. Adding a nonlinearity to the signal, for instance a second harmonic in the forcing function as is the case during MET operation, does not seem to change the result as seen in Figure 25 (right). However, adding an interruption to the signal does seem to change the behavior and make it look like some force traces observed (Figure 26, left). These interruptions could happen at any time or frequency due to the changing driving conditions, and have been observed in experiments shown in the varying beam vibration during the sweeps or the fixed frequency tests. Moreover, the larger second harmonic vibration of the brass mass at resonance, as compared to the aluminum vibration, is another indication of nonlinear vibration. That nonlinearity could be generated due to the rubber pad, or loosening of the screws on the bracket side where stainless steel screws grip the softer brass material. Second harmonic vibration could also be explained by stick-slip of the screw connection. The possibility of a nonlinear spring connection due to the stick-slip of the screws was simulated by applying a sinusoidal function to the spring stiffness, which is a rough approximation of the effect [39]. In Figure 26 (right), the results of the simulation with the nonlinearity in the spring shows that a net displacement of the beam could be obtained if the sinusoidal forcing function was in phase with the stick-slip of the screws, resulting in a shift in the center of mass on the balance beam during the pulse.

Lastly, the idea of a shifting center of mass on a torsion balance that results in a false positive has been previously examined by Ciomperlik using a linear actuator on a similar torsion balance [40]. To compensate the center of mass shift of the device on the beam, the resting position of the beam slightly changes. If the shift is permanent, caused by vibration or slipping of one or more screws for example, the force trace results in an offset in the force trace, as is even observed in CSUF publications [6]. It is also possible for the device to engender a center of mass shift during particular vibration modes, and a FEM analysis could be conducted to illustrate these modes, but the model would also need to include nonlinearity and it is beyond the scope of this paper. Thermal expansion effects due to rapid heating in the piezo-ceramic stack or brass mass at certain resonances are not excluded, but vibrations can explain the non-linear behavior observed.

7. Conclusion

The multitude of experimental campaigns, and support from CSUF has led to a good understanding of the MEGA drive's electromechanical system, and the observation of force traces similar to the ones in the literature on a torsion balance in vacuum. The effects observed are switching transients that reverse according to the device orientation, as well as a small quasi-static component for a pulse at a fixed driving frequency. The observed effect for a fixed frequency, however, is two orders of magnitude lower than Woodward's claimed effect, even when trying to pin-point the optimal frequency at resonance, or at the occurrence of maximal second harmonic content. Likewise, the switching transients are observed in the 90° orientation of the device as well. Effects with larger order of magnitude are observed when sweeping the driving frequency with fine steps, however, this effect is also observed with the device in the 90° orientation, which disagrees with the theory of uniaxial thrust. The observed force also does not seem to depend greatly on the frequency, driving voltage and second harmonic as the theory suggests. Finally, low-frequency beam vibration was observed in all device orientations, at resonance, and was observed to come and go as the driving conditions change during a fixed frequency pulse and sweeps, especially at switch-on, and despite measures taken to damp the vibrations. Hence, the effects observed by Woodward using the MEGA drive on a torsion balance can be explained by thermal and vibrational artefacts using Newtonian mechanics.

Acknowledgements

We gratefully acknowledge the support for SpaceDrive by the German National Space Agency DLR (Deutsches Zentrum für Luft- und Raumfahrttechnik) by funding from the Federal Ministry of Economic Affairs and Energy (BMWi) by approval from German Parliament (50RS1704). The authors are grateful to the Centre for Information Services and High Performance Computing (Zentrum für Informationsdienste und Hochleistungsrechnen (ZIH)) TU Dresden for providing its facilities for high throughput calculations, and to the Fraunhofer Institute for Ceramic Technologies and Systems IKTS (Institut für Keramische Technologien und Systeme) for providing its facilities for impedance spectrometry. We would also like to acknowledge the support from J. Heisig, J. Woodward and H. Fearn for their contributions to the ongoing experiments.

References

[1] J.F. Woodward, A new experimental approach to Mach's principle and relativistic gravitation, Found. Phys. Lett. 3 (1990) 497–506.

[2] J.F. Woodward, Making Starships and Stargates: The Science of Interstellar Transport and Absurdly Benign Wormholes, Springer, New York, 2013. https://doi.org/10.1007/978-1-4614-5623-0.

[3] J.F. Woodward, A stationary apparent weight shift from a transient Machian mass fluctuation, Found. Phys. Lett. 5 (1992) 425–442. https://doi.org/10.1007/BF00690424.

[4] H. Fearn, Experimental tests of the Mach Effect Thruster, in: Proc. Int. Astronaut. Congr. IAC, 2014.

[5] L.L. Williams, N. Inan, Maxwellian mirages in general relativity, (2020). http://arxiv.org/abs/2012.08077.

[6] H. Fearn, J.F. Woodward, New Experimental Results for Mach Effect Gravitation Assist (MEGA) drives, in: AIAA Propuls. Energy Forum NNF, Indianapolis, 2019. https://doi.org/10.2514/6.2019-4285.

[7] M. Kößling, M. Monette, M. Weikert, M. Tajmar, The SpaceDrive project - Thrust balance development and new measurements of the Mach-Effect and EMDrive Thrusters, Acta Astronaut. 161 (2019) 139–152. https://doi.org/10.1016/j.actaastro.2019.05.020.

[8] K. Nordtvedt, Existence of the gravitomagnetic interaction, Int. J. Theor. Phys. 27 (1988) 1395–1404. https://doi.org/10.1007/BF00671317.

[9] D. Sciama, On the Origin of Inertia, Cambridge, 1953.

[10] J.F. Woodward, Method for Transiently Altering the Mass of Objects to Facilitate their Transport or Change their Stationary Apparent Weights, 5,280,864, 1992.

[11] A. Wolff, D. Cramer, H. Heliebrand, C. Schuh, T. Steinkopff, K. Lubitz, Energy considerations of PZT multilayer actuators under dynamic driving conditions, Appl. Ferroelectr. 1996. ISAF '96., Proc. Tenth IEEE Int. Symp. 1 (1996) 317–320 vol.1. https://doi.org/10.1109/ISAF.1996.602758.

[12] J.J.A. Rodal, A Machian wave effect in conformal , scalar – tensor gravitational theory, Gen. Relativ. Gravit. 51 (2019) 1–23. https://doi.org/10.1007/s10714-019-2547-9.

[13] D.W. Sciama, P.C. Waylen, R.C. Gilman, Generally covariant integral formulation of Einstein's field equations, Phys. Rev. 187 (1969) 1762–1766. https://doi.org/10.1103/PhysRev.187.1762.

[14] C.H. Brans, Absence of inertial induction in general relativity, Phys. Rev. Lett. 39 (1977) 856–857. https://doi.org/10.1103/PhysRevLett.39.856.

[15] H. Fearn, A. Zachar, K. Wanser, J. Woodward, Theory of a Mach Effect Thruster I, J. Mod. Phys. 6 (2015) 1510–1525.

[16] H. Fearn, N. van Rossum, K. Wanser, J.F. Woodward, Theory of a Mach Effect Thruster II, J. Mod. Phys. 06 (2015) 1868–1880. https://doi.org/10.4236/jmp.2015.613192.

[17] J.F. Woodward, A laboratory test of Mach's Principle and strong-field relativistic gravity, Found. Phys. Lett. 9 (1996).

[18] J.F. Woodward, Flux capacitors and the origin of inertia, Found. Phys. 34 (2004) 1475–1514.

[19] N. Buldrini, M. Tajmar, K. Marhold, B. Seifert, Experimental Results of the Woodward Effect on a uN Thrust Balance, in: AIAA/ASME/SAE/ASEE Jt. Propuls. Conf. Exhib., 2006: pp. 1–12. https://doi.org/10.2514/6.2006-4911.

[20] H. Fearn, N. van Rossum, K. Wanser, J.F. Woodward, Theory of a Mach Effect Thruster II, J. Mod. Phys. (2015) 1–15.

[21] M. Tajmar, Mach-Effect thruster model, Acta Astronaut. 141 (2017) 8–16. https://doi.org/10.1016/j.actaastro.2017.09.021.

[22] A. Abdullah, M. Shahini, A. Pak, An approach to design a high power piezoelectric ultrasonic transducer, J. Electroceramics. 22 (2009) 369–382. https://doi.org/10.1007/s10832-007-9408-8.

[23] J.F. Woodward, D. Kennifick, M. Broyles, C. Akins, H. Fearn, J. Rodal, P. March, Mach Effects for In-

Space Propulsion: Interstellar Mission - NIAC Phase II Final Report, Los Angeles, 2020. https://www.nasa.gov/directorates/spacetech/niac/2018_Phase_I_Phase_II/Mach_Effect_for_In_Space_Propulsion_Interstellar_Mission/.
[24] N. Buldrini, Verification of the thrust signature of a Mach effect device, Wiener Neustadt, 2014.
[25] M. Tajmar, M. Kößling, M. Weikert, M. Monette, The SpaceDrive Project - First Results on EMDrive and Mach-Effect Thrusters, (2018).
[26] M. Monette, M. Kößling, M. Tajmar, The SpaceDrive Project - Progress in the Investigation of the Mach-Effect-Thruster Experiment, in: 36th Int. Electr. Propuls. Conf., 2019: pp. 15–20.
[27] H. Fearn, J. Woodward, Recent Results of an Investigation of Mach Effect Thrusters, in: 48th AIAA/ASME/SAE/ASEE Jt. Propuls. Conf. Exhib., American Institute of Aeronautics and Astronautics, Reston, Virigina, 2012. https://doi.org/10.2514/6.2012-3861.
[28] H. Fearn, J.F. Woodward, New Experimental Results of the Mach Effect Gravitational Assist (MEGA) Drive, in: AIAA Propuls. Energy Forum NNF, Indianapolis, 2019: pp. 1–12. https://doi.org/10.2514/6.2019-4285.
[29] Attocube Systems AG, Displacement sensor, one dimensional interferometer with nanometer accuracy, (2019). www.attocube/en/products.
[30] Carvin, Carvin Engineering Data: Operating Manual DCM1000, n.d.
[31] PI Ceramics, Piezoelectric Actuators: Components, Technologies, Operation, 2012.
[32] SKF Group, SKF Linear Motion & Precision Technologies, Bolt-tightening Handbook, 2001. https://studylib.net/doc/18040987/bolt-tightening-handbook.
[33] K. Uchino, Introduction to Piezoelectric Actuators and Transducers, Penn State University Park, 2003.
[34] F. Li, L. Jin, Z. Xu, S. Zhang, Electrostrictive effect in ferroelectrics : An alternative approach to improve piezoelectricity, Appl. Phys. Rev. 1 (2014). https://doi.org/10.1063/1.4861260.
[35] D. Guyomar, N. Aurelle, L. Eyraud, Piezoelectric Ceramics Nonlinear Behavior. Application to Langevin Transducer, J. Phys. III. 7 (1997) 1197–1208. https://doi.org/10.1051/jp3:1997183.
[36] B.K. Mukherjee, W. Ren, S.-F. Liu, A.J. Masys, G. Yang, Non-Linear Constitutive Properties of Piezoelectric Ceramics, MRS Proc. 276 (1992) 41–54. https://doi.org/10.1557/proc-276-39.
[37] W. Jiang, W. Cao, Nonlinear properties of lead zirconate – titanate piezoceramics, 88 (2000). https://doi.org/10.1063/1.1325384.
[38] H. Fearn, Private communication, (2020).
[39] C. Gao, D. Kuhlmann-Wilsdorf, D.D. Makel, The Dynamic Analysis of Stick-slip Motion, Wear. (1994) 1–12.
[40] J. Ciomperlik, False-Positive Thrust Signals from Center-of-Mass Offsets on a Fullerton-Style Thrust Balance, 2020. https://forum.nasaspaceflight.com/index.php?action=dlattach;topic=48855.0;attach=1948005.

Tables

Table 1: Thrust balance comparison

Parameters	C-Flex Bearing	Arm Length [cm]	Beam Moment of Inertia [$kg \cdot m^2$]	Balance Natural Period [s]	Background Noise [nN]
CSUF	E-10	19	0.05	5	100
TUD	A-20	35	0.17	8	20

Table 2: MET device comparison

Parameters	Brass Mass Dia. (mm)	Brass Mass Length (mm)	Alu. Mass Dia. (mm)	Alu. Mass Length (mm)	Stack Length (mm)	Stack Dia. (mm)	Stack Screw	Bracket Screw
NS5/NS7	28.5	19	28.5	4.7	18	19	2-56*	4-40*
WT3	28.9	19	28.9	3.9	18	19	2-56*	4-40*

***These are the UNC Thread ANSI standards**

Figures

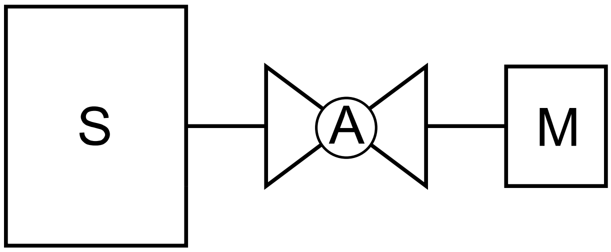

Figure 1: Woodard's conceptual design for an MET

An actuator (A) attached to a large spacecraft (S) pushes and pulls a mass (M) undergoing mass fluctuation to produce static thrust

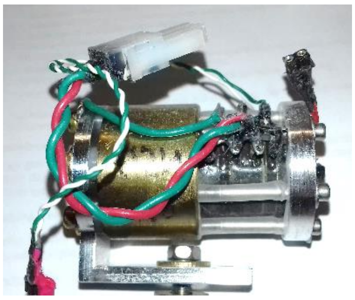

Figure 2: Current embodiment of the MET/MEGA Drive [20]

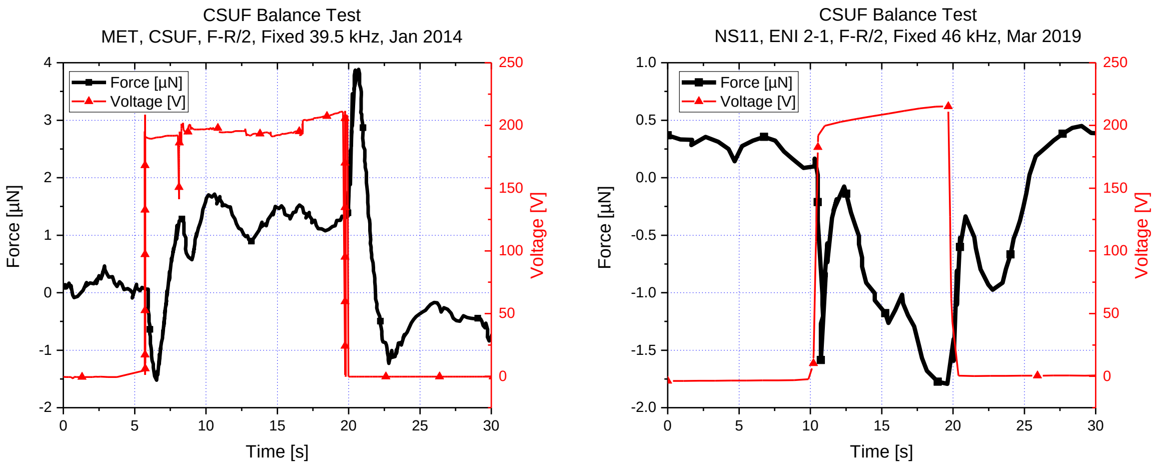

Figure 3: MET balance test results from CSUF

Left: net results (forward-reverse/2), driving frequency of 39.5 kHz, Carvin amplifier and transformer, Right: net results (forward-reverse/2), driving frequency of 46 kHz, ENI amplifier and transformer Data from Woodward[6,15]

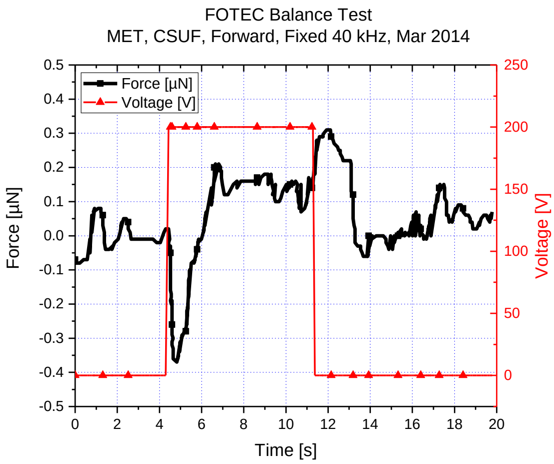

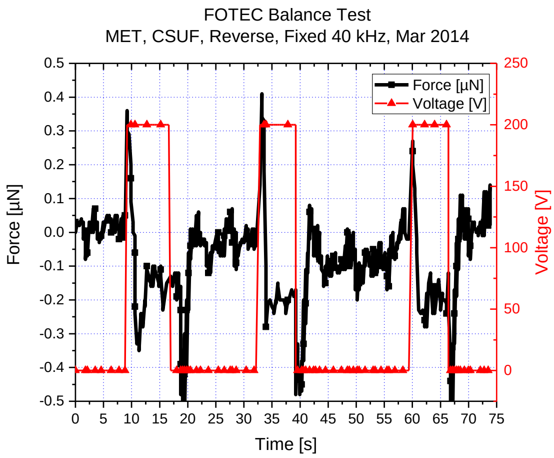

Figure 4: MET drive balance test results from FOTEC

Left: forward results, driving frequency of 40 kHz, Carvin amplifier and transformer,
Right: reverse results, driving frequency of 40 kHz, Carvin amplifier and transformer
Data from Buldrini [24]

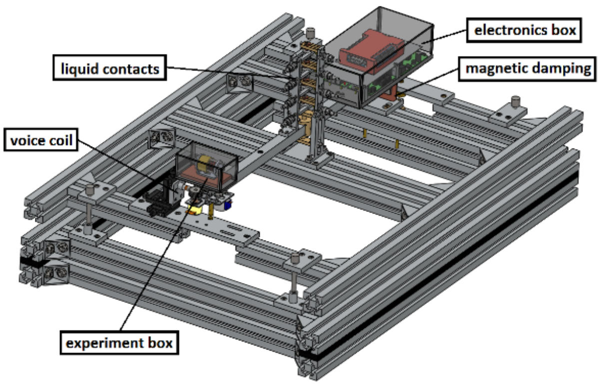

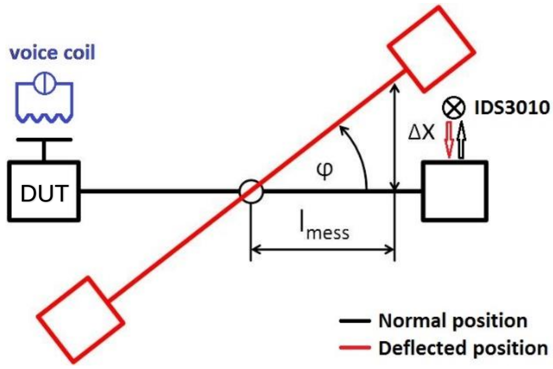

Figure 5: CAD model and sketch of the torsion balance (V6)

Left: CAD rendering of the torsion balance showing parts descriptions,
Right: 2D sketch and top view of the torsion balance with device-under-test (DUT)

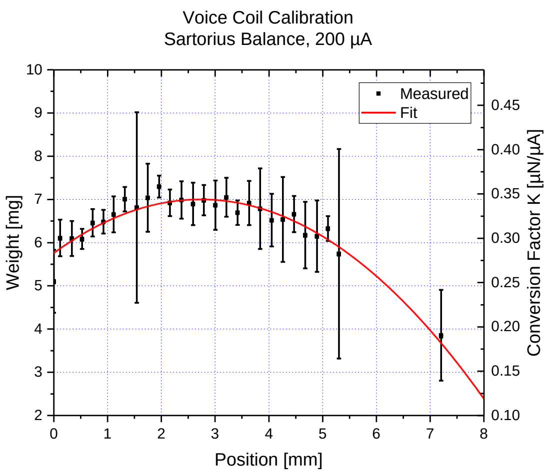

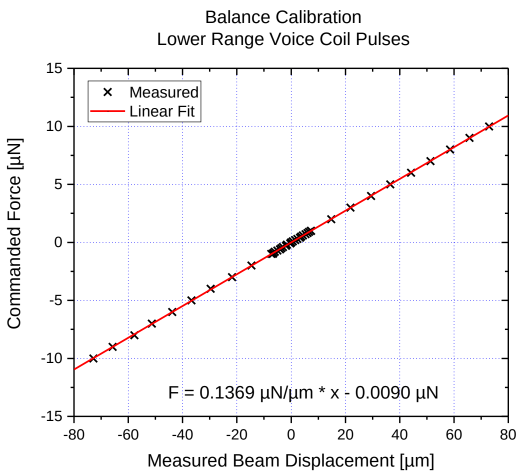

Figure 6: Typical calibration curves of the voice coil and balance

Left: voice coil calibration using the Sartorius balance and varying the magnet to solenoid gap
Right: balance calibration using a selection of voice coil pulses

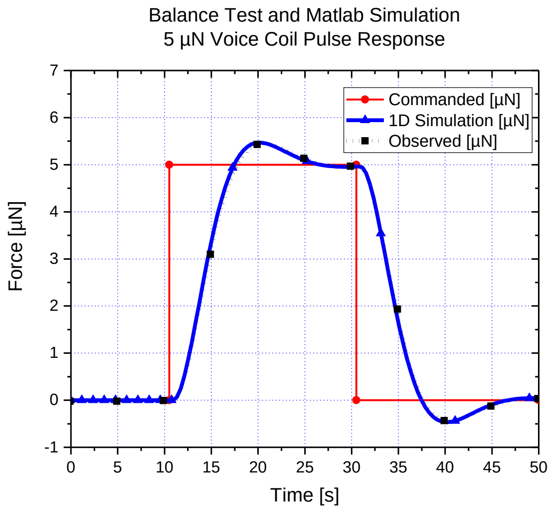

Figure 7: Pulse response of the balance with 1D simulation superposition

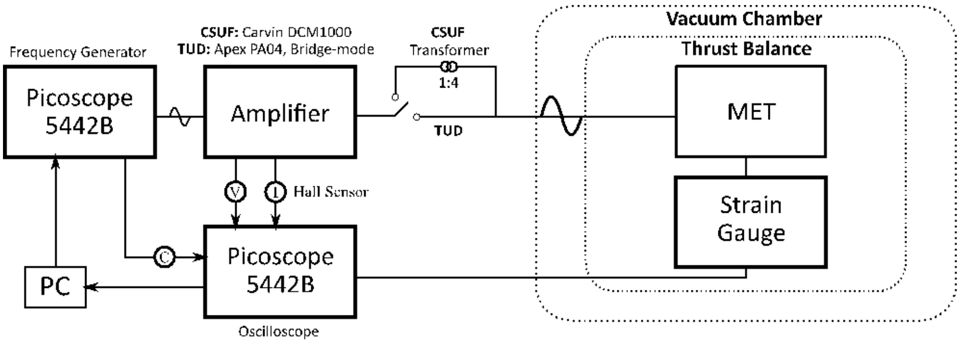

Figure 8: Block diagrams of TUD and CSUF electronics

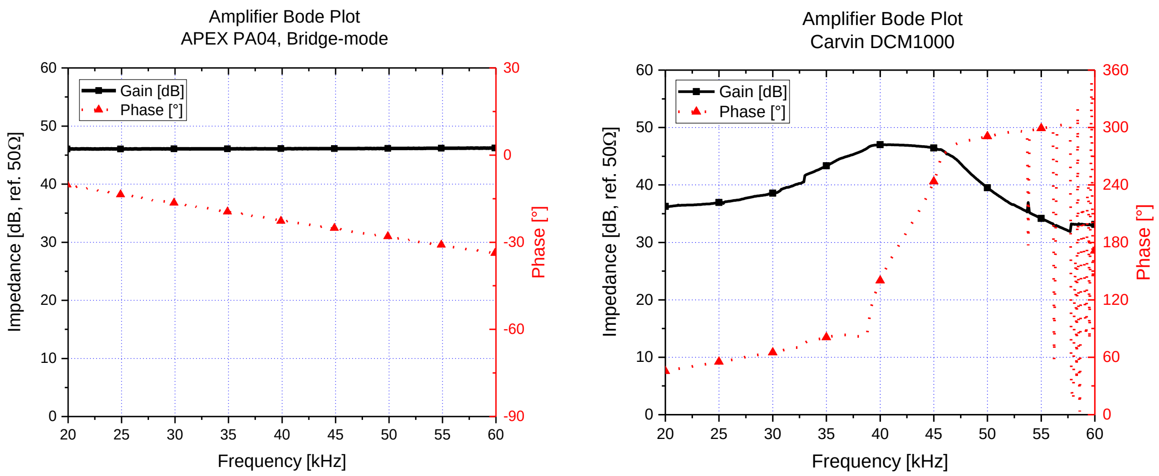

Figure 9: Bode plots of both amplifiers
Left: TUD electronics, Right: CSUF electronics

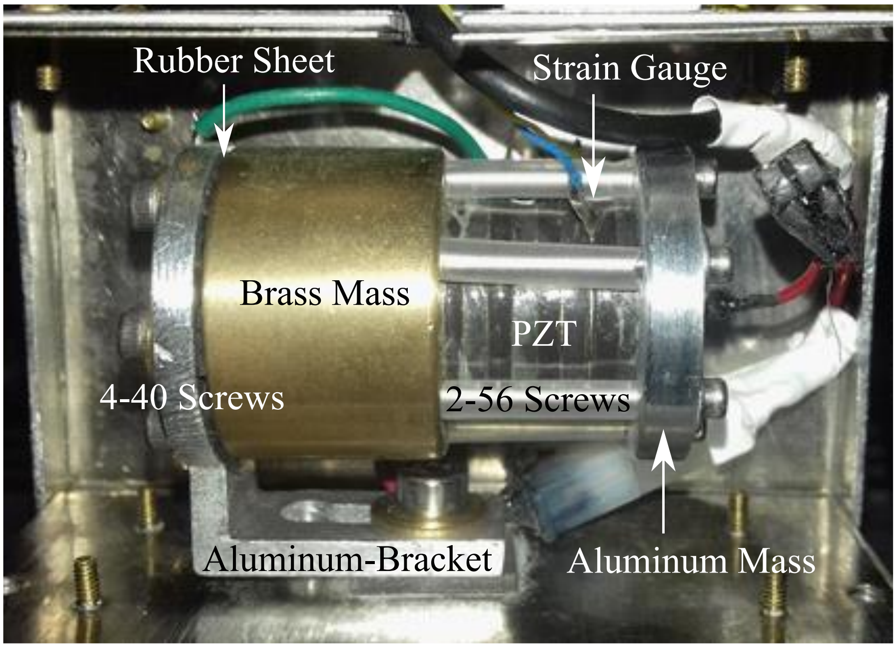

Figure 10: Description of the MET device (NS5)

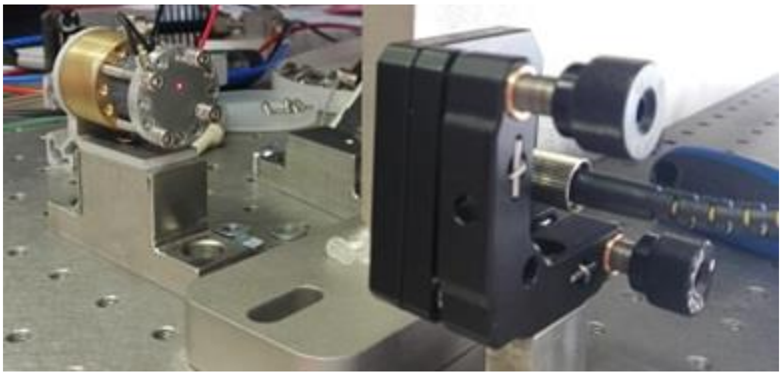

Figure 11: Picture of the vibration test setup

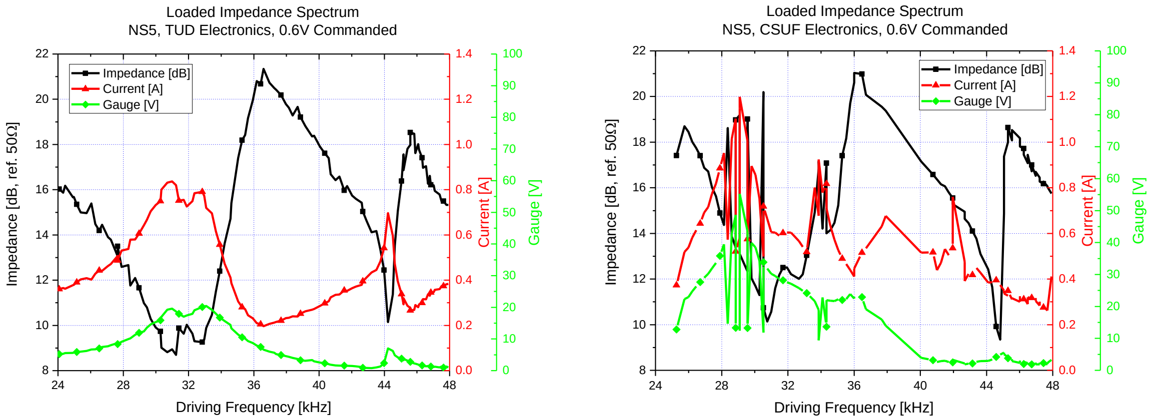

Figure 12: Loaded MET frequency spectra

Left: NS5 loaded spectrum (TUD) showing impedance, strain gauge signal and current

Right: NS5 loaded spectrum (CSUF) showing impedance, strain gauge signal and current

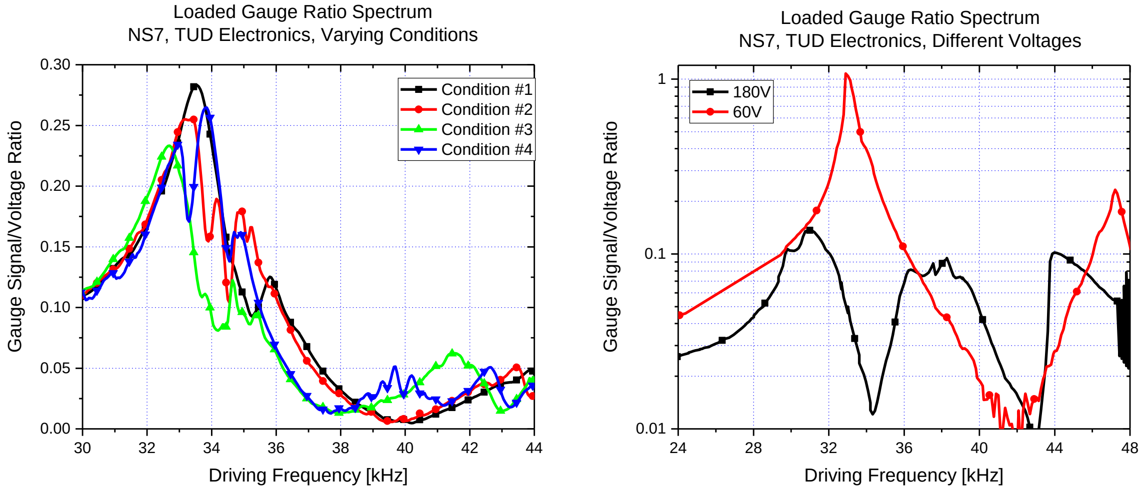

Conditions	Description
#1	Fixed to yoke and balance. Room temperature and atmosphere (30/09/19)
#2	Fixed to yoke and balance. Room temperature and vacuum (01/10/19)
#3	Fixed to yoke and balance. After pulse series, 43°C and vacuum (02/10/19)
#4	Fixed to yoke and balance. After cool-down, room temperature and vacuum (04/10/2019)

Figure 13: Strain gauge signal spectra

Left: strain gauge signal spectra of device NS7, unloaded, and in different conditions and timestamps
Right: strain gauge signal spectra of device NS7, loaded (TUD), with varying voltage

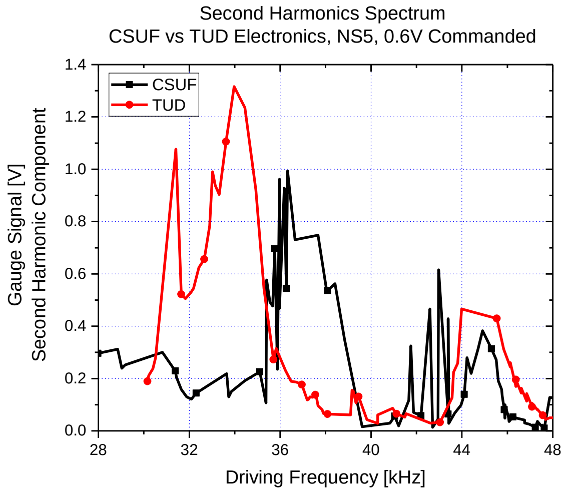

Figure 14: Second harmonic in driving voltage frequency sweeps

Second harmonic signals obtained through FFT are plotted against the driving frequency

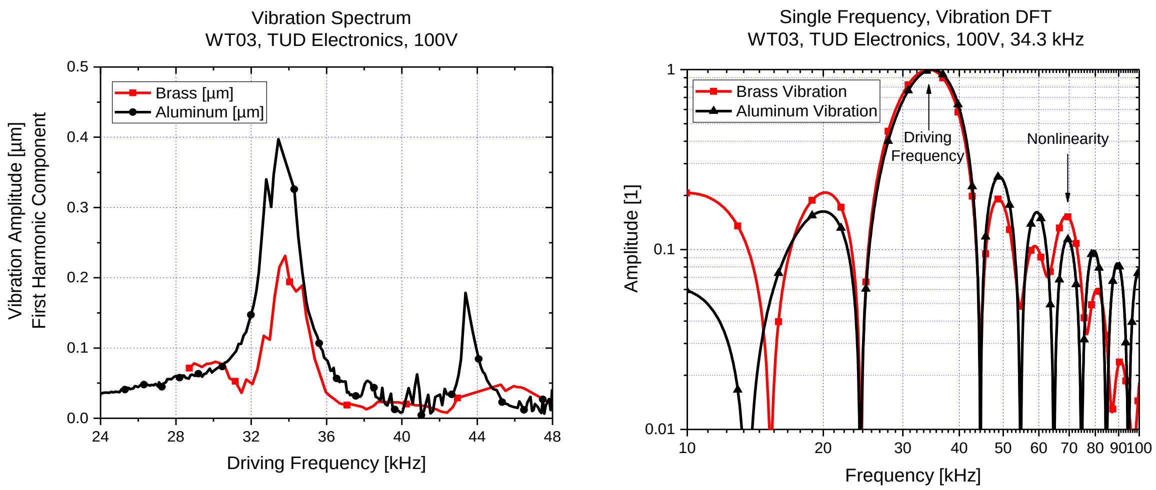

Figure 15: Vibration test results

Left: compares the vibration of brass and aluminum masses obtained in a driving frequency sweep
Right: shows a DFT of the aluminum and brass masses' vibration at a driving frequency of 34.3 kHz

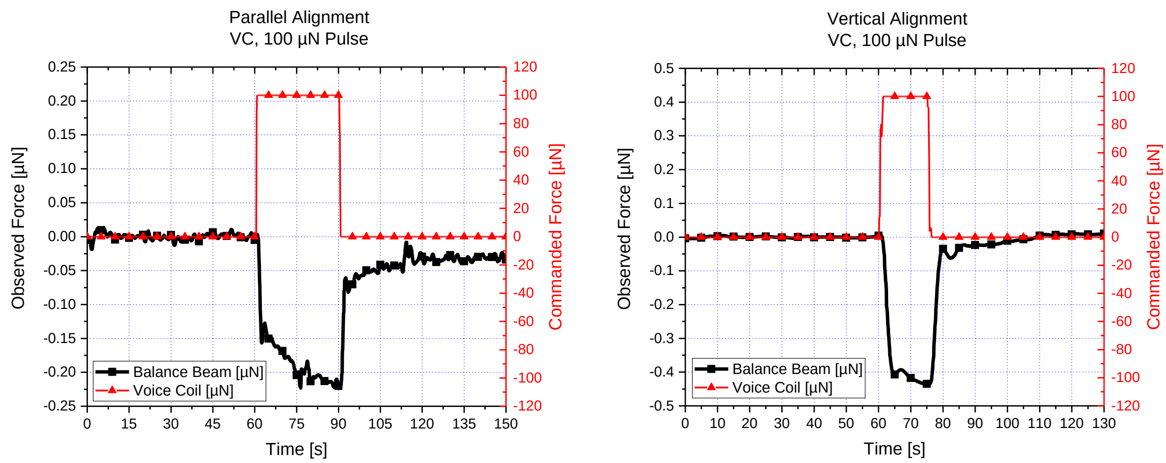

Figure 16: Voice coil calibration pulses in off-thrust axes

Left: the voice coil pulls the balance beam longitudinally and generates a small negative displacement
Right: the voice coil pulls the balance beam upwards and generates a small negative displacement

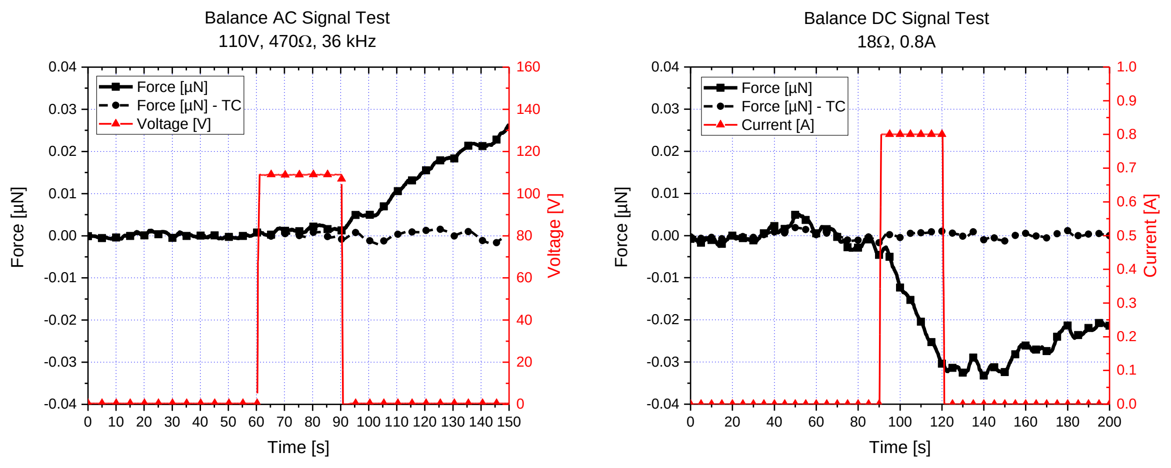

Figure 17: AC and DC dummy resistor test results

Left: AC signal test with 110V and low current, Right: DC signal test with 0.8A and low voltage. The dashed line indicates a thermally compensated force trace (TC).

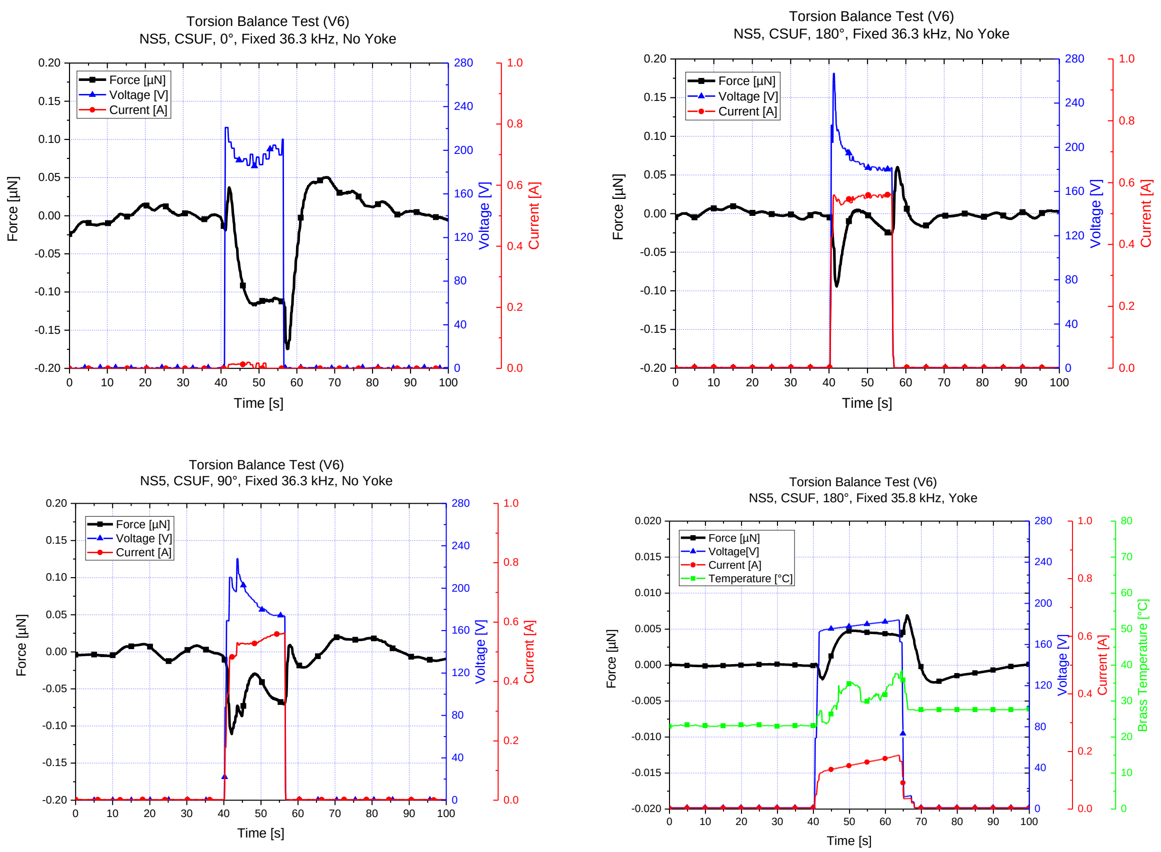

Figure 18: NS5 fixed frequency pulse results, CSUF electronics

Top left: 0° orientation without yoke and failed current measurement, top right: 180° orientation without yoke, bottom left: 90° orientation without yoke, bottom right: 180° orientation with yoke. All tests are conducted with a fixed frequency of 36.3 kHz during a 16 s pulse (except for bottom right: 24 s pulse, 35.8 kHz). The force traces are thermally compensated.

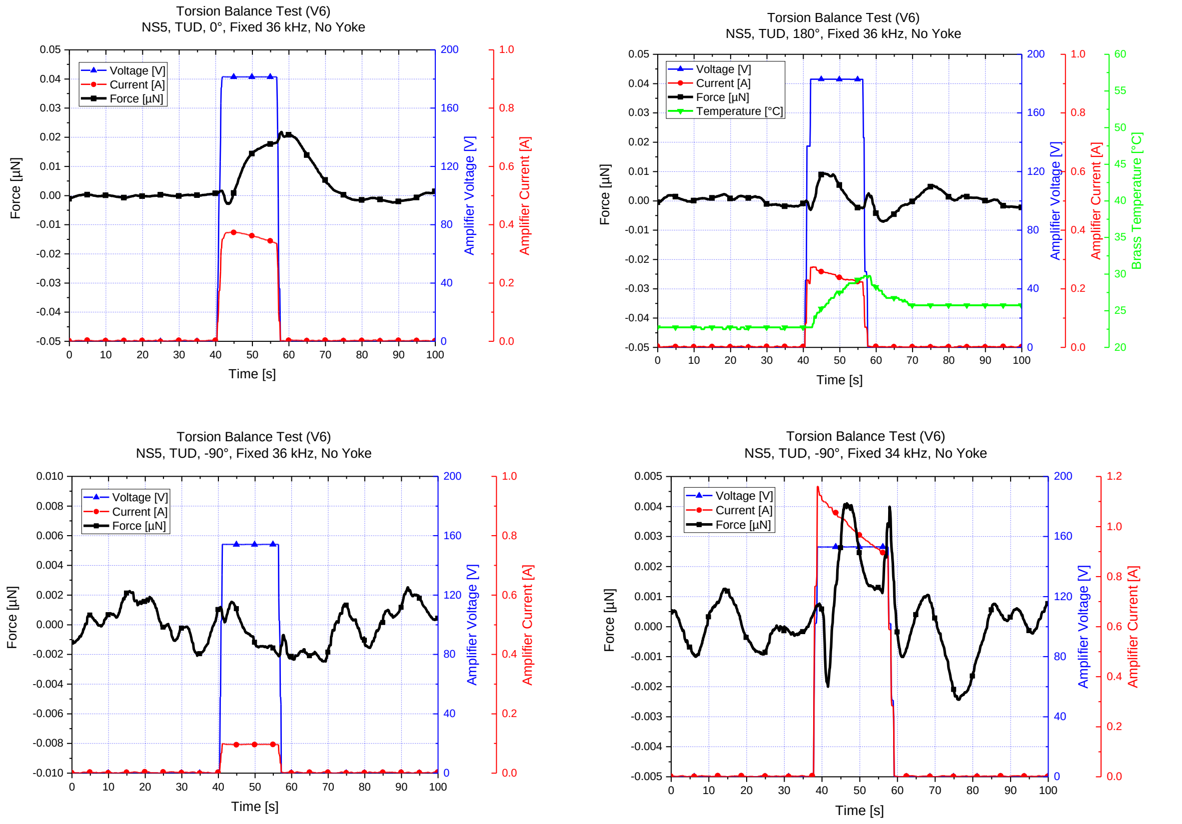

Figure 19: NS5 fixed frequency pulse result, TUD electronics

Top left: 0° orientation, top right: 180° orientation, bottom left: -90° orientation, similar to 90° orientation but with the device rotated 360° so that the brass mass is closer to the balance center, bottom right: -90° orientation again. All tests are conducted with a fixed frequency of 36.3 kHz during a 16 s pulse (except for bottom right: 16 s, 34.0 kHz). The force traces are thermally compensated.

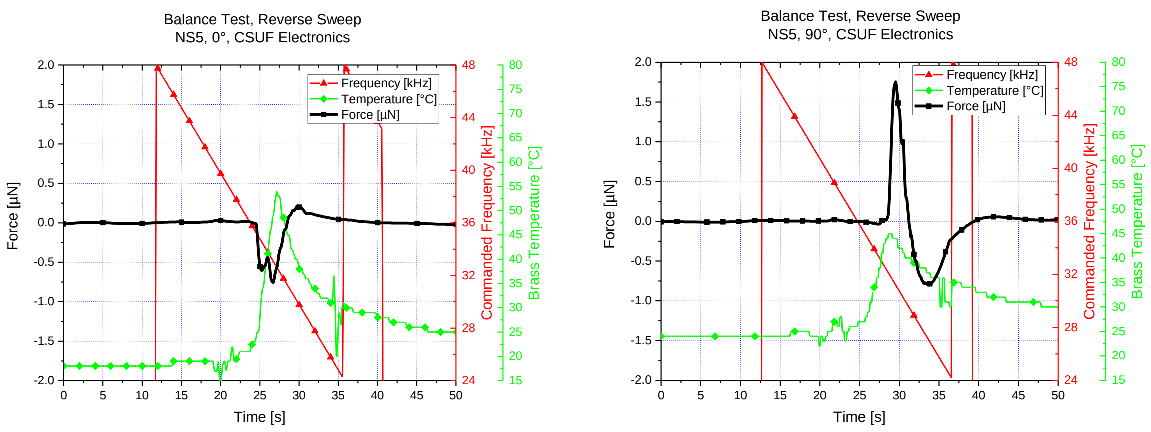

Figure 20: CSUF sweep at 0°, sweep at 90° with current and observed force

0° (left) and 90° (right) orientation tests with the driving frequency being swept backwards from 48 to 24 kHz. The force traces are thermally compensated.

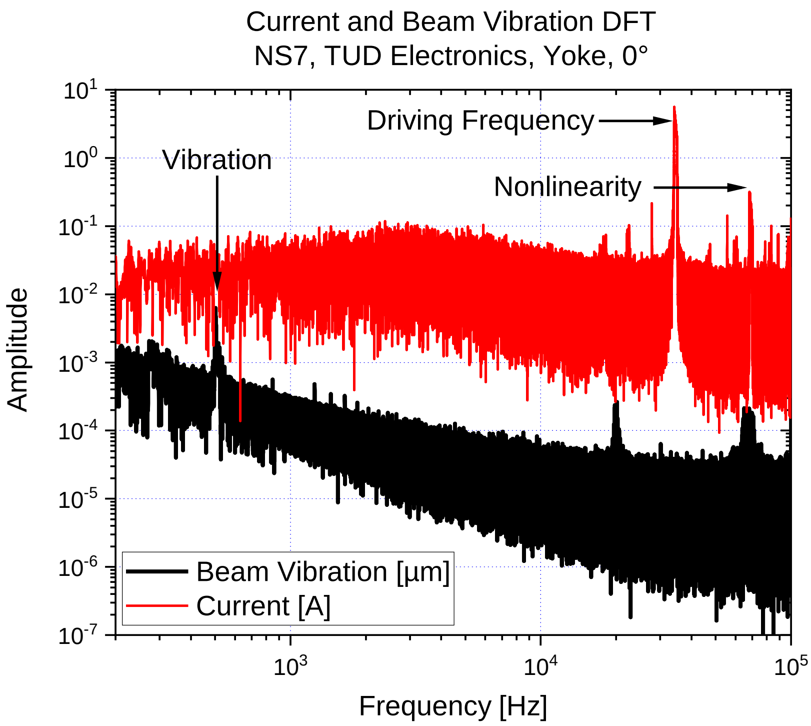

Figure 21: Single waveform beam vibration and current DFT

Illustrates the DFT of current and beam displacement at a high sampling rate (200 kHz) and at a specific driving frequency (35 kHz)

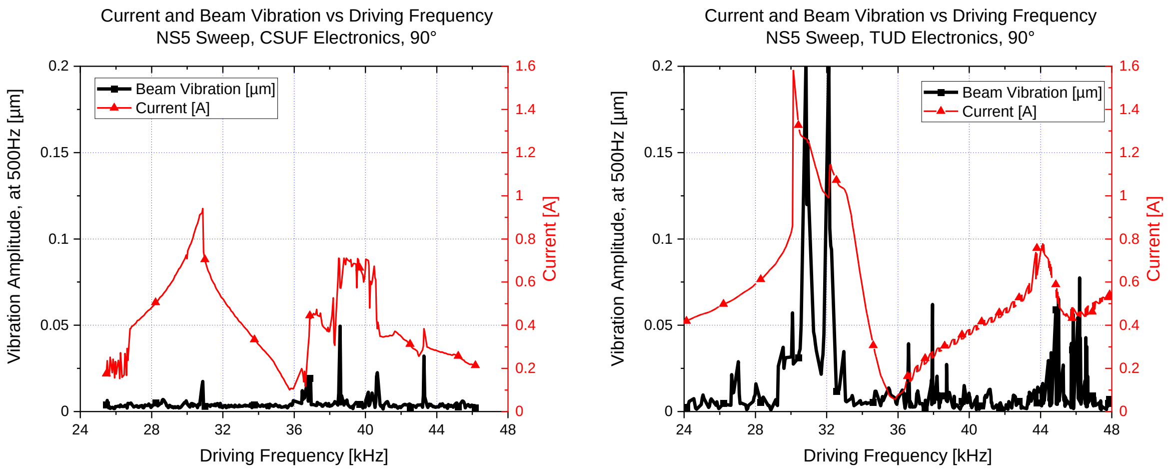

Figure 22: DFT of voltage sweeps and resulting beam deflection at 500 Hz

The graphs show the vibration amplitude component at 500 Hz, which was observed as a large sub-harmonic component during these backwards driving frequency sweeps. The sweeps go from 48 to 24 kHz, with the MET in the 90° orientation, and using CSUF (left) and TUD electronics (right)

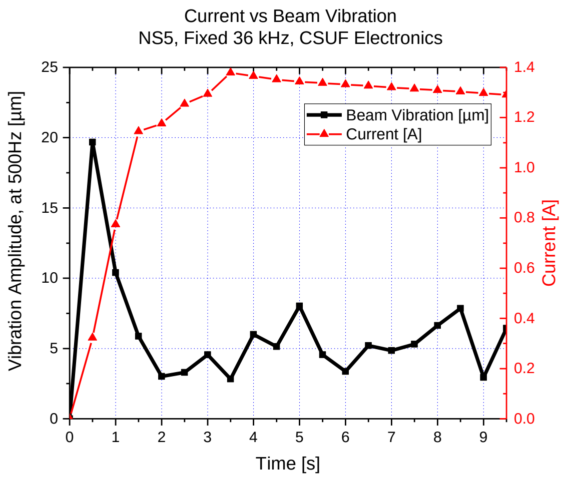

Figure 23: DFT of fixed frequency driving current and resulting beam deflection

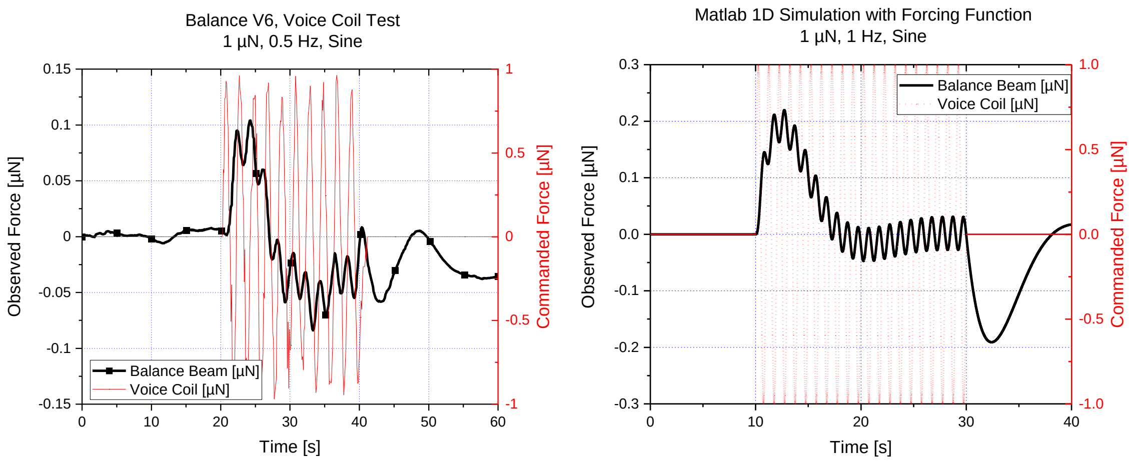

Figure 24: Pulse test results with forcing function and beam displacement
Left: experimental test result using the voice coil 0.5 Hz on the torsion balance
Right: Matlab 1D simulation result using a 1 µN pulse and a forcing frequency of 1 Hz

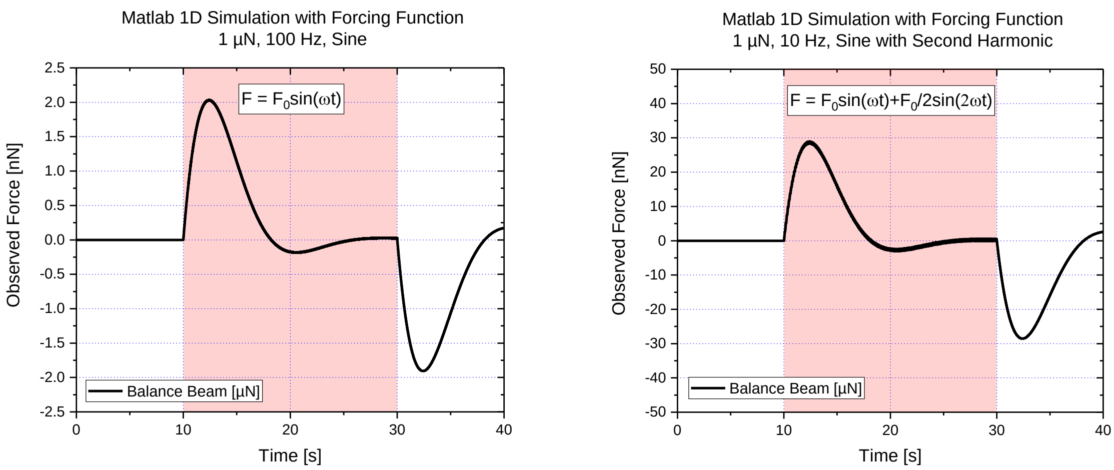

Figure 25: 1D balance model and linear forcing simulation results
Left: Matlab 1D simulation result using a 1 µN pulse and a forcing frequency of 100 Hz
Right: Matlab 1D simulation result using a 1 µN pulse and combined frequency components of 10 and 20 Hz
The shaded region indicates the time segments where the forcing function is active.

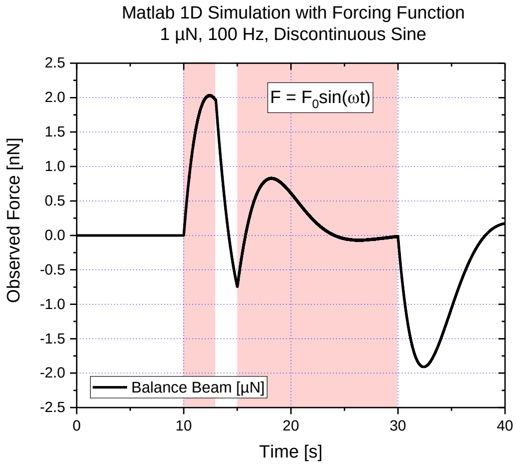

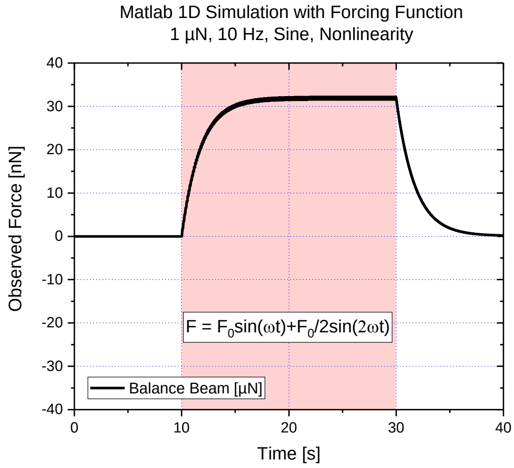

Figure 26: 1D balance model and nonlinear forcing simulation results

Left: simulation result with a 10 Hz forcing function with non-linearity in spring constant
Right: simulation result with a 100 Hz forcing function with intermittent switching,
The shaded region indicates the time segments where the forcing function is active.